The preservation of last-glacial (>50 to 40 ka) colluvium on low-relief surfaces in Alishan, an actively uplifting mountain in southwestern Taiwan

Meng-Long Hsieh [a,] *,
Alan Hogg [b],
Su-Chen Kang [c],
Chun-Yen Chou [c],

[a] Department of Earth and Environmental Sciences, National Chung Cheng University, Chiayi, Taiwan.
[b] Radiocarbon Dating Laboratory, University of Waikato, Hamilton, New Zealand.
[c] Department of Geosciences, National Taiwan University, Taipei, Taiwan.

*Corresponding author:
Tel: 886-6-52720411x66222
E-mail: hsiehml@ntu.edu.tw
Address: Department of Earth and Environmental Sciences, National Chung Cheng University, 168 University Road, Minhsiung Township, Chiayi County 62102, Taiwan, ROC

The preservation of last-glacial (>50 to 40 ka) colluvium on low-relief surfaces in Alishan, an actively uplifting mountain in southwestern Taiwan

Abstract

Geomorphic studies on the Taiwan orogen have long focused on the rapid erosion and efficient sediment transport in response to active tectonic uplift and frequent earthquakes/heavy rains. Little attention has been paid to the common low-relief surfaces in high mountains that appear to have been geomorphically stable for a long period of time. We undertook a study on a group of such gentle surfaces in Alishan, which consist of poorly drained hummocky slopes averaging 15° and as wide as 2 km. These gentle slopes are underlain by mass-wasting gravels 60 – 100 m thick, from which 22 radiocarbon dates >50 to 40 ka BP in age were obtained. Below these thick colluvial deposits are ~20° bedrock bedding planes apparently exposed by dip-slope failures. Combining these data reveals alternating hillslope erosion and deposition, along with episodic river downcutting, at a time scale of several 10^4 yr. We relate this temporal change in geomorphic processes to glacial-interglacial climate change. During the wet inter-/post-glacial periods characterized by frequent heavy rains, landslides/debris flows prevailed and rivers were capable of conveying most sediment eroded from hillslopes. Frequent debris flows combined with sufficient bedload sediments serving as tools for fluvial erosion caused rapid river downcutting. In

contrast, the low river erosion/transport capacity during the dry last-glacial period allowed progressive deposition of thick colluvium on the preexisting, gentle bedding surfaces probably eroded during the last interglacial period. This study shows how glacial-interglacial climate change influenced the river/hillslope processes and landscape evolution of the Taiwan orogen.

[Key words: Low-relief surface, Climate change, Landslide, Taiwan orogen]

1. Introduction

The Taiwan orogen (Fig. 1) has been considered an example of non-glaciated mountain belts with the tectonic uplift balanced by erosion, achieving a topographic steady state, with elevations limited to 4000 m despite eroding rapidly for millions of years (Suppe, 1981; Willett et al., 2003; Stolar et al., 2007). Geomorphic studies of Taiwan's mountains, influenced by this perception and with clear evidence of the strong impact of earthquakes/heavy rains, have long emphasized the rapid erosion and efficient sediment transport on steep slopes (e.g., Hovius et al., 2000; Dadson et al., 2003; Lin et al., 2009) and along bedrock rivers (e.g., Hartshorn et al., 2002; Schaller et al., 2005; Yanites et al., 2010; Cook et al., 2013). However, little attention has been paid to the common gentle topographies exhibiting rounded crests, hummocky slopes, alluvial surfaces, or low-gradient meandering channels stranded in high mountains

that appear to have been geomorphically stable for a long period of time. These low-relief, high-elevation topographies (or surfaces) were recognized by Japanese researchers a century ago (Lin, 1957). In that era, dominated by Davis's *cycle of erosion* (Davis, 1899), the juxtaposition of these gentle surfaces with surrounding steep slopes was believed indicative of alternate cessation and rejuvenation of tectonism that drove episodic river planation and downward incision, respectively (Lin, 1957). Since then, and long after the decline of Davis's theory, no additional hypotheses have been proposed to address the origin of these landscapes.

Perhaps the main reason why these low-relief, high-elevation surfaces have long been ignored is the scarcity of outcrops to study. In addition, most of these topographies are located in remote inaccessible areas. So far, neither constitutive nor chronological data of these landscapes have been reported.

This study explores in detail for the first time low-relief topographies in the high mountains of Taiwan, focusing on the Alishan area (Fig. 1). The area is known for its large stretches of conifer forests, including one of the most famous tourist attractions in Taiwan: the Alishan forest recreation park (hereafter the Alishan Park). The forests consisted of numerous, very large red cypress trees, evidence of the millennial geomorphic stability of the area. It was not until the erosion brought by Typhoon Morakot in 2009 that some deep-seated colluvium was exposed. We examined the

77 sedimentary features of this colluvium and obtained >30 radiocarbon dates. These,
78 along with the topographic features, allowed us to reconstruct landscape histories,
79 estimate bedrock incision rates, and interpret their significance. Most of the dates
80 obtained are >40 ka. They are expressed as radiocarbon ages (designated BP). The
81 remaining dates (<7 ka) are converted to 1σ calibrated age ranges (designated cal BP)
82 and calibrated using the Bayesian calibration programme OxCal (Rev 7.0.4, Bronk
83 Ramsey, 2001, 2009) utilizing the Northern Hemisphere calibration curve IntCal 13
84 (Reimer et al., 2013). Although this study focuses on landscape evolution at a local
85 site, the results help us understand how climate changes at glacial-interglacial scales
86 could control mass-wasting and fluvial processes in shaping active mountains like
87 Taiwan.
88
89 **2. Study area**
90 *2.1. Geological and geomorphic settings*
91 The Alishan, located west of the Yushan (at 3952 m, the highest elevation in
92 Taiwan), refers to the <3000-m high mountain area from which the
93 Chinshui/Chenyeolan rivers flow to the north and the Tsengwen River to the south
94 (Fig. 1). The area is underlain by Miocene shallow marine sedimentary rocks. The
95 younger Kuantoushan sandstone and the older Nanchuan formation (sandstone/shale)

96 strike generally southwest and dip 10 – 30° to the north (Fig. 2). As a part of the
97 Taiwan orogen, the tectonic uplift of the area started no earlier than ~5 million years
98 ago (e.g., Teng, 1990). Based on apatite fission-track dating from the Chenyeolan
99 River ~10 km north of the study area (Fuller et al., 2006), the denudation rate of the
100 region is estimated to be 2 – 4 mm yr^{-1} in the past 1 – 2 million years. The area is
101 currently uplifted at rates up to 14 mm yr^{-1} (mostly >8 mm yr^{-1}), according to leveling
102 surveys across its southern part (Fig. 2) (Ching et al., 2011).

103 The attitude of the rock formations apparently controls the topography of the
104 region, as almost all of the hillslopes dipping north or west are much wider and
105 gentler than those dipping south or east (Figs. 3 and 4). These relatively gentle slopes
106 can be grouped into two broad, low-relief surfaces, the Tashan surface in the north
107 and the Alishan surface in the south, separated by the Alishan River, the upstream
108 portion of the Chinshui River (Figs. 3 and 4). The Tashan surface, underlain by the
109 Kuantoushan sandstone, includes some abandoned alluvial surfaces and is deeply
110 dissected by rivers flowing to the north. The Alishan surface (Figs. 5a and b),
111 underlain by the Nanchuan formation, is characterized by poorly drained hummocky
112 slopes of apparently mass-wasting origin. This study focuses on the Alishan surface
113 and its bounding Alishan River, as they offered better exposures to study.

114 The Tashan surface is bounded to the south by a prominent cliff, the Tashan cliff,

115 along the north bank of the Alishan River (Figs. 3 and 4). This cliff exhibits multiple
116 landslide scarps cutting the thick Kuantoushan sandstone and is 700 – 1000 m high
117 where it fringes the ridge connecting Mt. Datashan (2663 m) and Mt. Tashan (2484 m)
118 of the Tashan surface (Figs. 5c and d). A truncated valley serving as the headwaters of
119 a north-flowing river cutting the Tashan surface exists on this ridge (Fig. 3).
120 The Alishan has a monsoon climate and receives annual rainfall of 3000 – 5000
121 mm, most of which comes from summer monsoons or tropical typhoons that
122 commonly bring daily rainfalls of >500 mm. The area is also subject to fog cover
123 (>100 days per year), which facilitates the growth of Taiwan red cypress
124 (*Chamaecyparis formosensis*), a conifer with a long life span that formed impressive
125 forests of giant trees commonly 3 – 2 ka in age (e.g., Chan and Huang, 2015).
126 Logging of these forests began in the early twentieth century with the construction of
127 mountain railways for transportation. The logging ceased in 1965 and the forests have
128 been restored, with the railways used for tourism purposes.
129
130 *2.2. Recent geomorphic changes*
131 The 1999 Chichi earthquake (M_w = 7.6) occurring in central Taiwan destroyed the
132 main train station in the Alishan Park and triggered many landslides in the region. A
133 branch of the mountain railway system, the Mianyue railway, was cut by a landslide

134 from Datashan Mountain. More landslides and debris flows occurred after the
135 earthquake, mainly along the Tsengwen River and the lower/middle parts of the
136 Alishan River. The mass movements culminated during Typhoon Morakot (7 – 10
137 August, 2009), which delivered a record 2800 mm of rain in the area. The Mianyue
138 railway was cut again by a landslide (named the Datashan; Fig. 5d) generated from
139 the same site as the 1999 landslide. This landslide also produced debris flows
140 downslope along a tributary (labelled A) of the Alishan River (Fig. 3).
141 The largest landslide (named the Erhwanping) triggered by the 2009 typhoon in
142 Alishan took place at a north-dipping slope facing the Alishan River, drained by a
143 tributary labelled C (Fig. 3). This landslide, with the main scarp located close to the
144 ridge top, has a source area 600 – 700 m high, 800 m wide, and a volume of 1.3×10^7
145 m^3 (Lee et al., 2012). It damaged the train station of Erhwanping and, ~300 m below,
146 eroded away a 600 m-long section of the railway east of Pingthena train station (Fig.
147 6). A part of the landslide then ran along a relatively narrow valley before entering the
148 Alishan River and generating debris flows there (Figs. 3 and 6).
149 The Erhwanping is known as an area prone to landslides. The area is named for
150 its distinctive flat surface that had an area of 6.6×10^4 m^2 and served as a lumber
151 distribution center in the early twentieth century (Chen, 2008). This flat surface,
152 however, was reduced to ~5.6×10^4 m^2 by a rainfall-induced landslide in 1912. An

153 earthquake (Chungpu) in 1941 demolished the train station and caused the collapse of
154 the surface by 7×10^3 m^2. The 1999 Chichi earthquake did not cause erosion in the
155 area, but after the 2009 typhoon the surface was reduced to 1.7×10^4 m^2, a quarter of
156 its original area (Chen, 2008).

157 The 2009 typhoon triggered two additional notable landslides in the study area.
158 One, labelled X (Figs. 3 and 7), occurred southwest of Erhwanping, from the middle
159 part of a south-dipping slope facing the Tsengwen River. It eroded an area ~150 m
160 high, cutting the highway to the Alishan Park before running into a tributary of the
161 Tsengwen River (Fig. 7). Another landslide, labelled Y, was generated on a
162 north-dipping slope bounding the middle-lower course of the Alishan River (Figs. 3
163 and 7). The landslide was up to 250 m high and involved the failure of the entire
164 hillslope from the crest downward, depositing debris that formed a hummocky slope
165 at the toe. More minor landslides were generated, especially in the middle and lower
166 parts of the Alishan River catchment, with debris flows emanating from almost all
167 tributaries joining this part of the trunk river.

168

169 **3. The Alishan surface**

170 *3.1. Topography*

171 This group of hummocky surfaces comprises several parts separated by tributary

172 valleys or by relatively steep slopes >50 m high (Fig. 3). The broadest and the highest
173 surface (labelled S1), dipping northwestward from the divide between the Alishan and
174 Tsengwen rivers, encircles the uppermost part of the Alishan River (Fig. 7). It
175 comprises multiple hummocky surfaces bounded by arc-shaped scarps <30 m high
176 and has an average slope of 15°, which is somewhat gentler than the underlying
177 bedrock bedding planes nearby (dipping around 20°). The drainage networks on the
178 surface are commonly disconnected with ponds developed in local depressions
179 (including the scenic Sister Lake in the Alishan Park; Fig. 3). Continuous channels are
180 exhibited only on the lower parts of the surface. These channels incise the surface and
181 show prominent knickpoints where joining the trunk Alishan River.
182 To the west, a lower surface (labelled S2), including the area of Pingthena,
183 straddles the Alishan/Tsengwen drainage divide (Fig. 7). A large portion of this
184 surface facing the Alishan River was eroded away by the 2009 Erhwanping landslide,
185 which originated from the slope connecting this surface with the higher S1 surface.
186 Downslope from the eroded railway east of Pingthena, Surfaces S1 and S2 are
187 separated by a southeast-striking escarpment with Tributary C flowing along the base
188 (Figs. 3 and 5b). This escarpment exhibits thick sandstone beds, with some waterfall
189 steps developed along the lower part of Tributary C. Two major sets of nearly vertical
190 joints are shown, trending west-east and northwest-southeast. The former is parallel to

191 the Tashan cliff; the latter is consistent with the trend of the escarpment.

192 More hummocky surfaces, labelled S3, S4, and S5, are exhibited along the
193 northern side of the Tsengwen River (Fig. 3). Surfaces S3 and S4 are fringed to the
194 north with the main drainage divide by a cliff, which exhibits multiple landslide
195 scarps, like other cliffs in the study area. To the east and separated by a tributary
196 valley is Surface S5, which extends to the drainage divide with the Chenyeolan River.
197 Both the S4 and S5 surfaces are cut by some 50 – 100-m high, east-striking linear
198 escarpments (Fig. 3). It should be noted that although the regional hillslope dips to the
199 south, formed by the downward incision of the Tsengwen River, the hummocky
200 surfaces here dip generally to the west or northwest. Only the northern parts of
201 Surfaces S3 and S4 below the main drainage divide comprise south-dipping surfaces,
202 apparently formed by colluvial deposition (Fig. 7).

203

204 *3.2. Sedimentary features and chronology*

205 Giant boulders (or bedrock blocks), subangular to subrounded in shape and up to
206 several meters in diameter, are commonly found on the hummocky surfaces in the
207 study area. These surfaces are capped by poorly-stratified, yellow colored and
208 heavily-weathered colluvial gravels along gullies, roads, and railways entrenched into
209 the ground surface. The erosion brought by the 2009 landslides also revealed

remnants of lateritic soils and reddish colluvium underlying some slopes facing the Tsengwen River (Figs. 3 and 7). The reddish colluvium exposed along the scarp of Landslide X is commonly mixed with yellowish colluvium, with the red-colored muddy materials probably sourced from lateritic soils (Fig. 8). Many gravel clasts in these deposits also have been heavily weathered and can easily be scraped across concrete roads to produce red-colored streaks (Fig. 8c). Similar mixtures of yellowish and reddish gravels >20 m thick were also exposed where Landslide X cut Surface S2 in the downslope direction (Fig. 8d). Notably, no such reddish colluvium has been found in the Alishan River catchment.

The erosion by the 2009 landslides also revealed thick colluvial gravels below the hillslopes facing the Alishan River (Fig. 9). The Erhwanping landslide revealed that the site of Erhwanping train station (Surface S1) was underlain by colluvial gravels >60 m thick (Fig. 9a). Even the relatively steep source area of the landslide exhibited >50-m thick colluvium after the erosion by the landslide. The exposed colluvial gravels consist mostly of cobble- or boulder-sized clasts including angular to subrounded giant boulders. Most of these gravels are rich in grey-colored muds and exhibit matrix-supported textures (Fig. 9). Those below Erhwanping are ~20 m thick and show transitional boundaries with the surrounding yellowish gravels (Fig. 9a). The greyish gravels exposed upslope of Pingthena (>10 m thick) are truncated and

229 capped by yellowish, clast-supported gravels a few meters thick (Figs. 9b, c). All
230 these greyish gravels contain abundant, mostly non-carbonized, wood remnants (Fig.
231 9d). They have been dated 46,369±1389 BP at Erhwanping (Site 1, below Surface S1)
232 and >50 ka BP (seven dates) upslope of Pingthena (Sites 2 – 4, below Surface S2)
233 (Table 1; Figs. 6 and 7). Two of these >50 ka BP dates are derived from samples
234 collected on the surfaces of the Erhwanping landslide (Sites 3 and 4).
235 Similar greyish, wood-bearing gravels also outcropped below the lower part of
236 Surface S1, along a tributary (labelled B) of the Alishan River. They yielded four
237 dates, ranging from 45,548±1107 to 41,321±740 BP (Sites 5 and 6; Fig. 7). These
238 greyish gravels, like those constituting Surface S2 upslope of Pingthena, have a sharp
239 boundary with the overlying yellowish gravels (Fig. 9e). On the other side of the ridge
240 facing the Tsengwen River, patches of greyish gravels were exposed by a tributary
241 cutting Surface S3 as mixtures with yellowish gravels (Fig. 9f). Here, a date of >50 ka
242 BP was obtained (Site 7; Fig. 7).
243
244 **4. The Alishan River**
245 *4.1. Topography*
246 The Alishan River originates from Surface S1 and incises it deeply downstream
247 (Figs. 3 and 10). The uppermost part of the trunk river above the junction with

Tributary A, surrounded by dense forest, is characterized by cascade or step-pool topographies built typically by rounded, moss-veneered boulders up to 2 m in diameter (Fig. 11a). The river significantly steepens, with an accumulation of numerous subrounded giant boulders >2 m in diameter, near the mouth of Tributary A (Fig. 11b). From here to the tributary junction (~100 m long), the trunk river was dry during our visits when the weather was fine. In contrast, the lowermost part of Tributary A, gentler and covered by finer-grained gravels, constantly supplied running water to the trunk river. This tributary does not exhibit bedrock waterfalls at or near the river mouth, unlike others entering the upper/middle parts of the trunk river (e.g., Fig. 11c).

Along the lower part of Tributary A, an alluvial/colluvial terrace 10 – 50 m high is present (labelled T in Fig. 7), extending downstream to near the confluence with Tributary B. Farther downstream, a distinct waterfall ~20 m high is developed (labelled WF; Figs. 7 and 11d) along a river reach with more or less uniform bedrock lithology. Tributary C, which drains the area of the 2009 Erhwanping landslide, enters immediately downstream of this waterfall. From here to Landslide Y, the river flows mainly within a gorge (Fig. 11e). Above this gorge and opposite to the S2 surface, remnants of relatively gentle slopes are preserved along the lower part of the Tashan cliff (Figs. 7 and 11f). These slopes, higher than Surface S2 but lower than S1, appear

267 to have connected upslope with Surface S1 before the incision of the river (Fig. 10).
268 The river gradually widens after flowing out of the gorge and exhibits >50-m wide
269 floodplains with 10 – 50-m high terraces downstream from Laichi (Fig. 3).
270 During the 2009 typhoon, debris flows emanated from tributaries A, C, and
271 others entering the gorge portion of the trunk river. These debris flows left a series of
272 debris terraces (generally <10 m high), especially around the mouths of the tributaries
273 from which they emanated. Angular/subangular giant boulders, commonly >2 m in
274 diameter, were scattered along the river. Between the giant boulders were
275 finer-grained sandy/gravelly bars, chaotic or organized, apparently deposited by
276 minor debris flows or fluvial processes after the major debris-flow surges. All these
277 features are in great contrast with those along the uppermost part of the trunk river
278 above the junction with Tributary A.
279
280 *4.2. Sedimentary features and chronology*
281 Pre-2009 colluvial/alluvial gravels underlying hillslopes or terraces capped by
282 forests, outcropped extensively along the river. Bedrock, commonly separated from
283 the overlying colluvium by bedding planes (Fig. 11c), was only exposed downstream
284 from the middle point between the mouths of Tributaries A and B. The thickness of
285 the colluvial sediment below the outer part of Surface S1 is estimated as great as ~100

286 m, constrained by the heights of the exposed bedrock. The exposed bedrock generally
287 increased in height above the riverbed in the downstream direction. Along the gorge,
288 thick colluvial sediment was observed only at tributary mouths or within some
289 shallow embayments along the trunk river. However, high above the gorge, colluvial
290 gravels >50 m thick were found underlying the remnants of the gentle slopes stranded
291 along the lower part of the Tashan cliff (Fig. 11f).

292 A great portion of the exposed colluvial/alluvial gravels are grey in color (Figs.
293 12 and 13). Many of them contain abundant greyish mud and wood fragments, similar
294 to those exposed around Erhwanping and Pingthena. These distinct greyish gravels
295 have yielded multiple dates >40 ka. Four of them, ranging from 43,000±936 to
296 41,730±701 BP, were derived below the Datashan landslide, associated with the
297 proximal part of Terrace T (Site 9; Figs. 7 and 12a). Here, the terrace exhibited
298 bipartite sedimentary sequences. The lower part consists of massive, matrix-supported
299 greyish gravels ~20 m thick (Fig. 12b). The upper part, up to 30 m thick, comprises
300 fairly-stratified yellowish gravels intercalated with some greyish gravel sheets. The
301 four 44 – 41 ka BP dates were derived from the lower part. Immediately downstream
302 of the mouth of Tributary A, a date of 41,452±882 BP was obtained from the north
303 (right) bank of the trunk river (Site 10; Fig. 7). Two hundred meters downstream from
304 the junction with Tributary B (Site 12; Fig. 7), a block of greyish gravel on the

305 modern riverbed yielded a date of 46,295±1785 BP. More dates of >50 ka, >45 ka,
306 and 47,423±2820 BP, in an ascending stratigraphic order, were obtained below the
307 gentle-slope remnants fringing the lower part of the Tashan cliff, along a tributary
308 (labelled D) (Site 14; Figs. 7 and 12d).

309 In addition to the 44 – 41 ka BP dates, the proximal part of Terrace T also yielded
310 two dates of 6950 – 6860 and 6500 – 6450 cal BP (Site 9; Fig. 7), from the surface of
311 a scree slope emanating from the upper part of the terrace. The 6950 – 6860 cal BP
312 date was sampled from a large, partly carbonized wood fragment; the 6500 – 6450 cal
313 BP date, from a small non-carbonized wood piece within a block of greyish gravel.
314 Both samples must have been eroded from the upper part of the terrace, although their
315 corresponding stratigraphic positions are unclear. Three almost identical dates, 6490 –
316 6410, 6490 – 6410, and 6550 – 6460 cal BP, were also derived immediately
317 downstream of the mouth of Tributary A (Site 10; Figs. 7 and 12c), from the side of
318 the river opposite to where the 41,452±882 BP date was obtained.

319 The greyish gravels also yielded multiple dates <3 ka. One of them, 2750 – 2730
320 cal BP, was derived from the uppermost part of the trunk river, from a local terrace
321 (~5 m high) at the south (left) bank (Site 8; Fig. 7). A date of 900 – 740 cal BP was
322 obtained from a block of greyish gravel, ~300 m upstream of the junction with
323 Tributary B (Site 11; Fig. 7). At the lowest part of Tributary C, a date of 500 – 330 cal

BP was yielded from the base of a ~50-m thick gravel sequence apparently deposited by a pre-2009 landslide originating from Erhwanping (Site 13; Figs. 6 and 7). Within the gorge, dates younger than 1950 AD (i.e., containing bomb carbon) were obtained from three sites: a ~20-m thick gravelly debris-flow deposit at the mouth of Tributary D (Site 15; Fig. 7), a 2-m thick muddy sand bed stranded ~50-m high above the valley bottom (Site 16; Figs. 7 and 13a), and a >50 m-thick colluvial sequence 1.2 km farther downstream (Site 17; Figs. 7 and 13b).

Although no chronological data are available, the colluvial gravel exposed along the flank of Landslide Y is noteworthy (Fig. 13c). This landslide, leaving an extensive bedrock bedding plane (~30°) in the source area, is apparently of a dip-slope type (Fig. 13d). The western flank of the landslide cut bedrock, apparently following a set of nearly vertical joints trending northwest. The eastern flank of the landslide exhibited a wedge-shaped gravel mass that was up to 20 m thick at the toe of the slope and tapered off upward (Fig. 13d).

5. Synthesis and discussion

5.1. Mass-wasting histories

The existence of thick colluvial gravel has revealed ancient mass movements in the Alishan area. At least parts of these movements were deep-seated, supplying

343 enormous amounts of greyish, non-weathered clasts downslope. Debris flows were
344 involved, resulting in the deposition of disorganized gravels rich in muddy matrix.
345 The inclusion of abundant wood fragments in the debris-flow deposits implies
346 damage to forests. The incorporation of subrounded giant boulders, which are likely
347 to have been abraded in fluvial environments, suggests the destruction of drainage
348 networks. All these lines of evidence point to the catastrophic nature of the mass
349 movements. According to as many as 22 dates from multiple sites, these mass
350 movements occurred in a time period of >50 – 40 ka BP and, given the wide range of
351 the dates, probably included more than one event.

352 We recognize that 12 of the dates mentioned above, within 50 – 40 ka BP, are
353 close to the age limit of the radiocarbon dating methods. Considering the quantity of
354 the dates and that they are all derived from large wood samples, we believe these
355 dates are not significantly biased by contamination of modern carbon into the dated
356 samples, if any. The attainment of stratigraphically consistent dates from >50 ka to
357 47,423±2820 BP from a common profile below the Tashan cliff (Site 14; Fig. 7)
358 further reinforces the reliability of the dates and leads us to consider that all the >50
359 ka dates derived are probably only slightly beyond the age limit of the dating methods
360 (perhaps within 60 – 50 ka BP).

361 Our data imply that after 40 ka, erosion took place on the slopes facing the

362 Alishan River, resulting in the prevalence of erosional surfaces truncating the ≥40 ka
363 BP deposits. These erosional surfaces are all capped by relatively thin, yellowish
364 colluvium, which is likely to have been sourced from surficial, weathered clasts with
365 deposition rates lower than those of the gravels beneath. This suggests the mass
366 wasting that created the observed hummocky topographies on the studied gentle
367 surfaces occurred relatively slowly and/or infrequently.

368 Note that our dates (50 – 40 ka BP) obtained from the higher S1 surface are all
369 younger than those (>50 ka BP) from the S2 (Figs. 7 and 10). This implies that the
370 observed >50 – 40 ka BP mass-wasting sediment was deposited more or less
371 continuously, so that the strata exhibited at lower elevations are older than those at
372 higher elevations. The contrast between the elevations of the S1 and S2 surfaces then
373 requires that after the deposition, S2 was eroded and lowered more rapidly than S1.
374 This interpretation is consistent with the occurrence of the 2009 Erhwanping landslide,
375 which significantly lowered the S2 but not S1 (Fig. 7).

376 According to our data, it was not until 6.9 – 6.4 ka cal BP (more likely 6.5 – 6.4
377 ka cal BP) that mass movements from Mt. Datashan brought significant deposition
378 along the upper part of the Alishan River, forming Terrace T. Other mass-wasting
379 events (~2.7 ka and ~0.8 ka cal BP) are found along this part of the river, but their
380 resulting landforms and depositional records are minor.

381 The youngest mass-wasting events are all found along the middle-lower part of
382 the Alishan River. At the mouth of Tributary C, a ~0.4 ka landslide from Erhwanping
383 deposited gravelly colluvial deposits thicker than those brought by the 2009 event
384 (Fig. 6). In the downstream direction, a 50-m high sand bed is dated younger than AD
385 1950 (Site 16; Fig. 7). We consider this sand to have been deposited when the gorge
386 was dammed, with the deposition of the thick colluvium younger than AD 1950
387 downstream causing this damming (Site 17; Fig. 7). We suspect this event occurred
388 during the 1959 Tropical Storm 081 (August 7 – 9; induced by Typhoon Ellen), which
389 is second only to 2009 Typhoon Morakot in causing rainfall disasters in the recorded
390 histories of Taiwan.
391
392 *5.2. Controls of rock structures*
393 The control of bedrock structures on the hillslope morphology of Alishan is
394 shown by its asymmetric valley cross sections (Fig. 3). The processes shaping the
395 wider and gentler north-dipping slopes must have been different from those shaping
396 the slopes dipping south. The similarity in attitudes between the low-relief,
397 hummocky surfaces and the underlying bedrock bedding planes may suggest a
398 dip-slope origin for the surfaces. These surfaces are not typical of dip slopes however,
399 as they are underlain by colluvial sediments of great thicknesses. We believe this

400 characteristic reflects bidirectional roles of the observed bedding planes on hillslope
401 development. In conditions that the toes of hillslopes were cut, causing “daylight” of
402 bedding planes, dip-slope failures dominated. The existence of these movements is
403 manifested by the common appearance of bedding planes serving as boundaries
404 between bedrock and colluvium. On the other hand, once the erosion stopped, the
405 gentleness of the bedding planes (i.e., the former slide surfaces) facilitated sediment
406 accumulation, allowing the deposition of thick colluvium eroded from the upper parts
407 of hillslopes.

408 The existence of high-angle joints parallel to hillslope dips is also significant, as
409 they could serve as lateral boundaries of landslides such as that flanking Landslide Y
410 (Fig. 13d). The escarpment separating Surfaces S1 and S2 (Fig. 5b) is also likely to
411 have originated this way. Slope failures with lateral boundaries following such
412 high-angle joints created local depressions (i.e., accommodation) on hillslopes, which
413 could determine where the thickest colluvial sediments could accumulate.

414 Landslide Y provides an example of how the hillslope processes inferred above
415 may have operated (Fig. 13d). This landslide moved along a set of bedding planes
416 (~30°) and was flanked in the west by a nearly vertical joint. Parts of the landslide
417 debris ran into the river and was conveyed away by debris flows, with the remaining
418 debris deposited at the toe of the hillslope. It is possible that as long as the toe of the

hillslope remains uneroded, more and more sediment would be able to accumulate on the slide surface (bedding plane) to form a colluvial mass similar to that exposed along the eastern flank of the landslide. Note that the colluvial mass exhibited here thins upward and has a surface gentler than the bedrock bedding planes (Fig. 13d). This feature is consistent with the available data that the observed low-relief, hummocky surfaces appear to be slightly gentler than the underlying bedrock bedding planes.

Landslide Y is relatively small, however. For the broad S1 and S2 surfaces to be created, it would be necessary, over long time frames, for dip-slope movements from the north-dipping hillslopes to force the trunk Alishan River to shift to the north in association with the downward incision of the river. A positive feedback mechanism may have operated, as the north-dipping hillslopes, once enlarged, could generate more extensive dip-slope failures, which in turn enhanced the northward migration of the river to successively widen the hillslopes. The expansion of Surfaces S1 and S2 must have caused the retreat of the Tashan cliff, which concords with the presence of a truncated valley on the top of the cliff (Fig. 3). Nearly vertical joints parallel to the trunk Alishan River helps maintain the steepness of the cliff by rock fall and/or toppling. Apparently, mass movements occurring at this side of the valley were relatively small and had limited influences on the lateral migration of the river,

compared with the dip-slope failures on the opposite side, resulting in the overall asymmetric shape of the valley.

We believe that processes similar to those inferred above also operated in the Tsengwen River valley. Accordingly, through the northward trimming of the trunk Tsengwen River, Surfaces S3, S4, and S5 are likely to have been narrowed over time (Fig. 3). However, unlike the Taishan cliff, the cliff separating the S1 from the S3/S4 surfaces, along with the east-striking linear escarpments crossing S4 and S5, show no evidence of river cutting (Fig. 3). Therefore, these steep slopes could all originate from landslides or gravitational faulting following the nearly vertical, valley-parallel joints that prevail in the region. How these landslides (or faults) moved and their significance upon the formation of Surfaces S3, S4, and S5 remain unclear. Nevertheless, given that lateritic soils/colluvium were only found at this side of the ridge but not at the opposite side facing the Alishan River, the former hillslope appears to have been more geomorphically stable than the latter (i.e., the landslides or faults mentioned above might have been inactive for a long period of time).

5.3. Downward river incision

Rivers incised after the formation of the studied gentle, hummocky surfaces. The downstream increase in the heights of Surfaces S1 and S2 above the Alishan River

457 indicates that the lower-middle part of the river has incised more rapidly than its
458 upper part since the abandonment of the surfaces (Fig. 10). This is also true for
459 bedrock, as its local heights exhibited along the river also increase in the downstream
460 direction, especially along the waterfall (WF) upstream of the junction with Tributary
461 C (Fig. 11d). Notably, no bedrock has been exposed along much of the upper part of
462 the Alishan River, which yields a zero bedrock incision rate averaged over the past 40
463 ka, according to our dates (Sites 8 and 10; Fig. 7).

464 We attribute the observed spatial contrast in river incision rate to the contrast in
465 landslide/debris-flow activities. Specifically, the lower-middle part of the Alishan
466 River catchment is likely to have undergone more active landslides/debris flows than
467 the upper part of the catchment. Debris flows are known as agents in eroding bedrock
468 (e.g., Stock and Dietrich, 2006; Hsu et al., 2008; De Haas and Van Woerkom, 2016).
469 Also, both theoretical and experimental studies have shown that significant fluvial
470 bedrock incision can only occur where sufficient amounts of bedload sediments can
471 act as saltation-abrasion tools for the incision (Sklar and Dietrich, 2001, 2004). As
472 landslides/debris flows are the major sources of bedload sediments, the activity of
473 landslides/debris flows (and the characteristics of the clasts they yield) poses strong
474 controls on bedrock river incision, as simulated by Egholm et al. (2013). A positive
475 feedback mechanism might have been involved because once a river rapidly incises, it

476 destabilizes hillslopes (e.g., causing “daylight” of bedding planes), which in turn
477 promotes landslide/debris-flow activities and the yield of bedload sediments for
478 erosion.

479 Our inferred spatial contrast in mass-wasting activity is supported by modern
480 observations, as during the 2009 typhoon nearly all tributaries (including C and D)
481 joining the lower-middle part of the trunk Alishan River (but only Tributary A in the
482 upper part) yielded debris flows. The greater activity of landslides/debris flows in the
483 lower-middle part of the Alishan River catchment must have caused greater local
484 erosion, which is consistent with our interpretation that Surface S2 has been lowered
485 more rapidly than S1. In fact, the erosion of Surface S2 would contribute many
486 landslides/debris flows (e.g., the 2009 Erhwanping) to the trunk river downstream
487 from the junction with Tributary C. This satisfactorily explains why Waterfall WF, a
488 result of differential bedrock incision, is located immediately upstream of the junction
489 with Tributary C.

490 The strong coupling between landslides/debris flows and river morphology can
491 further be viewed in the landscapes along the uppermost part of the Alishan River
492 upstream from the junction with Tributary A. This part of the river, lacking recent
493 landslides/debris flows and having experienced inactive bedrock incision over the past
494 40 ka, is characterized by cascade or step-pool topographies formed by rounded,

495 moss-veneered large boulders (Fig. 11a). These boulders appear to have been placed
496 by rock falls or landslides a long time ago, with more recent prevailing fluvial forcing
497 inadequate to emplace them. The significant increase in the sizes of the boulders
498 approaching the junction with Tributary A is due to the contribution of extremely
499 coarse clasts from Mt. Datashan. The accumulation of these giant boulders steepened
500 the trunk river and caused the water to flow underground (Fig. 11b). We believe that
501 these boulders can only be efficiently moved, and bedrock incised, by rare debris-flow
502 events like those emanating from Tributary A during the 2009 typhoon. In fact, with a
503 gentler slope and higher river flows, Tributary A was easily mistaken for the trunk
504 river in the field.
505
506 *5.4. The influence of glacial-interglacial climate change*
507 We have detected a temporal change in river/hillslope processes in the Alishan
508 area. The alternation of hillslope erosion and deposition has resulted in the deposition
509 of thick colluvial sediment overlying bedrock bedding planes. The episodic nature of
510 downward river incision created the landscape's gentle surfaces juxtaposed with steep
511 slopes. Note that the uppermost part of the Alishan River, fringed by the ~700-m high
512 Tashan cliff, has not been actively incised in the past 40 ka or longer. To compensate
513 for this morphological deficit, the river must have incised extremely rapidly before

514 the formation of Surfaces S1 and S2. The temporal change in the stability of the
515 landscape is also shown by the presence of reworked lateritic soils/gravels on
516 hillslopes. The minimum time period required for the development of lateritic soils, as
517 constrained by dates obtained elsewhere in Taiwan, has been inferred to be 30 – 20 ka
518 (Ota et al. 2002; Tsai et al., 2016). Our observed lateritic soils/gravels in Alishan,
519 which show much greater degree of lateralization than the 30 – 20 ka deposits, are
520 likely to have been developed for more than several tens of thousands of years. In
521 other words, before the emplacement of these heavily-weathered materials on
522 hillslopes, the study area had been geomorphically stable for at least several tens of
523 thousands of years, a time span consistent with the radiocarbon dates.

524 The chronological data mentioned above reveal that the detected changes in the
525 mode/rate of river/hillslope processes occurred at a time scale of several tens of
526 thousands of years. No evidence suggests a change in tectonic/seismic activities
527 during this time span. It is more likely the observed varying geomorphic processes
528 reflect the contrast between the glacial and interglacial climate conditions. Like the
529 monsoon-controlled paleoclimate in East Asian (e.g., An. 2000; Maher, 2016), the
530 glacial climate in Taiwan is characterized by cool and dry conditions, compared with
531 the climate during the interglacial and postglacial (Holocene) periods (Liew et al.,
532 2006). We propose that the thick colluvial deposits exposed in the study area were

533 deposited in the last-glacial time when the drier climate resulted in a low frequency of
534 landslides/debris flows and low river erosion/transport capability. In contrast, during
535 the wet inter-/post-glacial periods characterized by more frequent heavy rains, rivers
536 were able to flush out most of the sediment eroded from hillslopes (by both fluvial
537 and debris-flow processes), in conjunction with rapid downward incision that
538 steepened hillslopes and enhanced the potential for mass wasting (Fig. 14).

539 The characteristics of river/hillslope processes during the inter-/post-glacial
540 periods in Taiwan can be determined through observation of modern environments.
541 Only some extremely large heavy rainfall events triggered large-scale
542 landslides/debris flows. Other heavy rains that did not cause significant hillslope
543 erosion generated floods that scoured river banks and removed sediments deposited
544 during former slope failures. Because of this, only a few mass-wasting events could
545 have their stratigraphic/morphological evidence survive for more than a decade. Not
546 surprisingly, only limited Holocene fluvial and mass-wasting records were found in
547 the study area.

548 The monitoring of modern fluvial morphological changes in Taiwan shows that
549 torrents generated by heavy rains are capable of incising bedrock at rates up to
550 centimeters per year (Hartshorn et al., 2002) or even meters per event (Cook et al.,
551 2013), through conveying sufficient bedload sediment. Dating of Holocene river

552 terraces also yields bedrock incision rates up to a few centimeters per year (Schaller et
553 al., 2005; Hsieh et al., 2014). All these rates are apparently higher than the
554 contemporary tectonic uplift rates. We believe that the Holocene bedrock incision
555 rates along the lower-middle part of the Alishan River, especially the gorge area, are
556 no lower than the values mentioned above, considering that this relatively steep river
557 reach has been incised by not only fluvial but also debris-flow agents.

558 Our work indicates that in contrast to the modern environment, heavy rainfall
559 along with landslides/debris flows occurred relatively infrequently under glacial
560 conditions in Taiwan. We suggest that during this period, and especially between
561 landslide/debris-flow events, rivers typically had insufficient power to convey or
562 erode sediment residing on riverbeds or along banks. This condition was enhanced,
563 and the residence time of sediment increased, where landslides/debris flows supplied
564 oversized boulders to protect riverbeds, as shown along the uppermost part of the
565 Alishan River. We believe this low river competence (and thus mobility) explains why
566 sediment transported by each landslide/debris flow, even though uncommon, was able
567 to progressively accumulate in valleys during glacial times.

568

569 *5.5. Implications for the genesis of low-relief, high-elevation topographies*

570 The formation of low-relief surfaces in non-glaciated mountains requires

long-term cessation of river downcutting, during which river planation and/or hillslope degradation dominated. Emphasizing the acceleration of river downcutting that stranded the low-relief surfaces in high mountains suggests a rejuvenation of tectonic uplift following the formation of the surfaces (e.g., Davis, 1899). Underlining the slowing of river downcutting that started the formation of the surfaces in already-rugged mountains implies a decrease of drainage areas due to river piracy, in a condition of consecutive tectonic uplift (Yang et al., 2015). This study, however, provides alternative thinking. We have shown that the Alishan surface, one of the broadest low-relief, high-elevation surfaces in the Taiwan orogen, has been created in the past several tens of thousands of years. Over this time period, our observed change in the river-downcutting rate apparently overwhelmed any change of tectonic rates. No evidence of river piracy is shown in the studied landscapes. Also, the extensive colluvial aggradation that formed the Alishan surface could hardly be justified simply by the stability of tectonism or river piracy. Combination of these arguments suggests that the creation of this surface relates to glacial/interglacial climate change, an interpretation similar to that proposed by Oguchi et al. (2001) to explain the common downslope steepening of hillslopes in the mountains of Japan which have tectonic and geomorphic settings like Taiwan.

A key aspect of our interpretation is that over the time span of several tens of

590 thousands of years, downward river incision was mainly controlled by the frequency
591 of landslides/debris flows and their supply of bedload sediments serving as tools for
592 fluvial erosion. When the activity of landslides/debris flows was significantly lower,
593 river downcutting slowed down or even stopped, which facilitated the formation of
594 low-relief surfaces, even though the overall landscape was progressively raised by
595 tectonic uplift (Figs. 14d, e). In contrast, with frequent landslides/debris flows, river
596 downcutting significantly exceeded tectonic uplift, favoring the formation of steep
597 hillslopes (Figs. 14a – c). We argue that in the time scale indicated by this study, the
598 landslide/debris-flow activity and its influences on river processes can readily be
599 governed by climate forcing (e.g., magnitude/frequency of severe rains) without the
600 necessity of tectonic change or river network reorganization (e.g., river piracy).
601 We have suggested that the low-relief, high-elevation surfaces in Taiwan were
602 created during periods of low river mobility. Under this condition, the surfaces are
603 expected to have been shaped mainly by hillslope degradation, which could vary from
604 place to place in types/magnitudes, controlled by bedrock lithology and structures. In
605 Alishan, the broadness of both the Tashan and Alishan surfaces apparently reflects the
606 hardness and gentle dipping of the Kuantoushan sandstone and Nanchuan formation,
607 whose dips also determine the gradients of the two surfaces. The Alishan surface,
608 steeper and composed of more shale bedrock (Fig. 2), appears to have had greater

609 potential for large-scale dip-slope failures than the Tashan surface. It is through the
610 extensive deposition by this type of mass movement that we were able to obtain
611 datable materials to constrain the age of the surface and to shed light on the nature of
612 the low-relief, high-elevation surfaces in the orogen generally.
613
614 **6. Conclusion**
615 We have shown that at least parts of the gentle surfaces stranded in Alishan are
616 capped by mass-wasting gravels 60 – 100 m thick and dated >50 ka to 40 ka BP.
617 These thick colluvial deposits overlie surfaces composed of bedrock bedding planes
618 dipping ≤30°, apparently exposed by dip-slope failures. We propose this phase of
619 hillslope erosion occurred during the wet last-interglacial period when rivers were
620 capable of conveying most of the sediment eroded from hillslopes, in conjunction
621 with rapid incision facilitated by frequent debris flows and sufficient bedload
622 sediments serving as tools for fluvial erosion. In contrast, during the dry last-glacial
623 period the low erosion/transport capacity of rivers allowed the progressive deposition
624 of thick colluvium on the preexisting, relatively gentle bedrock bedding surfaces. It
625 was not until the postglacial period that frequent slope failures with rapid river
626 incision resumed, and the previously accumulated last-glacial colluvium started to be
627 flushed out of valleys.

This study demonstrates that the formation of one of the broadest gentle surfaces in the high mountains of Taiwan was strongly governed by glacial-interglacial climate change superimposed on long-term tectonic uplift. This conclusion provides a basis for future studies on erosion, sediment transport/residence histories, and the genesis of other low-relief, high-elevation topographies in the orogen in response to both tectonic and climate forces.

Acknowledgements

This research was sponsored by the Ministry of Science and Technology (ROC) (MOST 106-2116-M-194-014-010). We thank Dr. Lucas Mesalles in National Chung Cheng University for his valuable comments on the manuscript. Gratitude also goes to Mr. Yu-Da Xiao, Mr. Xiu-Guo Cui, Mr. Yi-Ho Tseng, and Miss Wan-Lin Hu from National Chung Cheng University for their kind help in the field survey.

References

An, Z.S., 2000. The history and variability of the East Asian paleomonsoon climate. Quaternary Science Reviews 19, 171 – 187.

Bronk Ramsey, C., 2001. Development of the radiocarbon calibration program OxCal. Radiocarbon 43, 355 – 363.

Bronk Ramsey, C., 2009. Bayesian analysis of radiocarbon dates. Radiocarbon 51, 337 – 360.

Chan, M.H., Huang, C.G., 2015. Tree ring and wood strength of veteran red cypress in Alishan, Taiwan. Quarterly Journal of Chinese Forestry 48, 263 – 282 (in Chinese).

Chen, Y.C., 2008. Memory of the Alishan landscapes: Erhwanping. Ecology Taiwan Quarterly 19, 49 – 53 (in Chinese).

Chinese Petroleum Corporation, 1986. Geological map of Chiayi, Chinese Petroleum Corporation, scale 1:100 000, 1 sheet.

Ching, K.E., Hsieh, M.L., Johnson, K.M., Chen, K.H., Rau. R.J., Yang, M., 2011. Modern vertical deformation rates and mountain building in Taiwan from precise leveling and continuous GPS observations, 2000-2008. J. Geophys. Res. 116, B08406, doi:10.1029/2011JB008242.

Cook, K.L., Turowski, J.M., Hovius, N., 2013. A demonstration of the importance of bedload transport for fluvial bedrock erosion and knickpoint propagation. Earth Surf. Process. Landforms 38, 683 – 695.

Dadson, S.L., Hovius, N., Chen, H., Brian Dade, W., Hsieh, M.L., Willett, S.D., Hu, J.C., Horng, M.J., Chen, M.C., Stark, C.P., Lague, D., Lin, J.C., 2003. Links between erosion, runoff variability and seismicity in the Taiwan orogeny. Nature

426, 648 – 651.

Davis, W.M., 1899. The geographic cycle. Geographical Journal 14, 481 – 504.

De Haas, T., Van Woerkom, T., 2016. Bed scour by debris flows: experimental investigation of effects of debris-flow composition. Earth Surf. Process. Landforms 41, 1951 – 1966.

Egholm, D.L., Knudsen, M.F., Sandiford, M., 2013. Lifespan of mountain ranges scaled by feedbacks between landsliding and erosion by rivers. Nature 498, 475–478, doi:10.1038/nature12218.

Fuller, C.W., Willett, S.D., Fisher, D., Lu, C.Y., 2006. A thermomechanical wedge model of Taiwan constrained by fission-track thermochronometry. Tectonophysics 425, 1 – 24.

Hartshorn, K., Hovius, N., Dade, W.B., Slingerland, R.L., 2002. Climate-driven bedrock incision in an active mountain belt. Science 297, 2036 – 2038.

Hovius, N., Stark, C.P., Chu, H.T., Lin, J.C., 2000. Supply and removal of sediment in a landslide-dominated mountain belt: Central Range, Taiwan. J. Geol. 108, 73 – 89.

Hsu, L., Dietrich, W.E., Sklar, L.S., 2008. Experimental study of bedrock erosion by granular flows. J. Geophys. Res.: Earth Surface 113, F02001, doi: 10.1029/2007JF000778.

685 Hsieh, M.L., Ching, K.E., Chyi, S.J., Kang, S.C., Chou, C.Y., 2014. Late Quaternary
686 mass-wasting records in the actively uplifting Pa-chang catchment, southwestern
687 Taiwan. Geomorphology 216, 125 – 140.
688 Lee, J.T., Ziao, D.K., Huang, C.R., Yang, H.Z., Shen, Y.C., 2012. The Investigation of
689 the Failure Mechanisms and Repair Planning of the Alishan Forest Railway.
690 Journal of Chinese Soil and Water Conservation 43, 123 – 138 (in Chinese).
691 Liew, P.M., Huang, S.U., Kuo, C.M., 2006. Pollen stratigraphy, vegetation and
692 environment of the last glacial and Holocene—A record from Toushe Basin,
693 central Taiwan. Quaternary International 147, 16 – 33.
694 Lin, C.C., 1957. Topography of Taiwan. Publication of the Taiwan Provincial
695 Documentary Committee, Taipei (in Chinese).
696 Lin, Z., Oguchi, T., Chen, Y.G., Saito, K., 2009. Constant-slope alluvial fans and
697 source basins in Taiwan. Geology 37, 787 – 790.
698 Maher, B.A., 2016. Palaeoclimatic records of the loess/palaeosol sequences of the
699 Chinese Loess Plateau. Quaternary Science Reviews 154, 23 – 84.
700 Oguchi, T., Saito, K., Kadomura, H., Grossman, M., 2001. Fluvial geomorphology
701 and paleohydrology in Japan. Geomorphology 39, 3 – 19.
702 Ota, Y., Bruce, H.D., Chen, Y.G., Hsieh, M.L., 2002. Deformation and age of fluvial
703 terraces south of the Choushui River, Central Taiwan, and their tectonic

704 implications. Western Pacific Earth Sciences 2, 251 – 260.
705 Reimer, P.J., Bard, E., Bayliss, A., Beck, J.W., Blackwell, P.G., Bronk Ramsey, C.,
706 Buck, C.E., Cheng, H., Edwards, R.L., Friedrich, M., Grootes, P.M., Guilderson,
707 T.P., Haflidason, H., Hajdas, I., Hatté, C., Heaton, T.J., Hoffmann, D.L., Hogg,
708 A.G., Hughen, K.A., Kaiser, K.F., Kromer, B., Manning, S.W., Niu, M., Reimer,
709 R.W., Richards, D.A., Scott, E.M., Southon, J.R., Staff, R.A., Turney, C.S.M.,
710 van der Plicht, J., 2013. IntCal13 and Marine13 radiocarbon age calibration
711 curves 0–50,000 years cal BP. Radiocarbon 55, 1869–1887, doi:
712 10.2458/azu_js_rc.55.16947.
713 Schaller, M., Hovius, N., Willett, S.D., Ivy-Ochs, S., Synal, H.A., Chen, M.C., 2005.
714 Fluvial bedrock incision in the active mountain belt of Taiwan from in-situ
715 produced cosmogenic nuclides. Earth Surf. Process. Landforms 30, 955 – 971.
716 Sklar, L., Dietrich, W.E., 2001. Sediment and rock strength controls on river incision
717 into bedrock. Geology 29, 1087 – 1090.
718 Sklar, L., Dietrich, W.E., 2004. A mechanistic model for river incision into bedrock
719 by saltating bed load. Water Resources Research 40,
720 doi:10.1029/2003WR002496.
721 Stock, J.D., Dietrich, W.E., 2006. Erosion of steepland valleys by debris flows. Geol.
722 Soc. Am. Bull. 118, 1125 – 1148.

723 Stolar, D.B., Willett, S.D., Montgomery, D.R., 2007. Characterization of topographic
724 steady state in Taiwan. Earth Planet. Sci. Lett. 261, 421 – 431.
725 Suppe, J., 1981. Mechanics of mountain building and metamorphism in Taiwan.
726 Memoirs of Geological Society of China 4, 67 – 89.
727 Teng, L.S., 1990. Geotectonic evolution of late Cenozoic arc continent collision in
728 Taiwan. Tectonophysics 183, 57 – 76.
729 Tsai, H., Hseu, Z.Y., Kuo, H.Y., Huang, W.S., Chen, Z.S., 2016. Soilscape of
730 west-central Taiwan: its pedogenesis and geomorphic implications.
731 Geomorphology 255, 81 – 94.
732 Willett, S.D., Fisher, D., Fuller, C., Yeh, E.C., Lu, C.Y., 2003. Erosion rates and
733 orogenic wedge kinematics in Taiwan inferred from apatite fission track
734 thermochronometry. Geology 31, 945 – 948.
735 Yang, R., Willett, S.D., Goren, L., 2015. In situ low-relief landscape formation as a
736 result of river network disruption. Nature 520, 526 – 529.
737 Yanites, B.J., Tucker, G.E., Mueller, K.J., Chen, Y.G., Wilcox, T., Huang, S.Y., Shi,
738 K.W., 2010. Incision and channel morphology across active structures along the
739 Peikang River, central Taiwan: implications for the importance of channel width.
740 Geol. Soc. Am. Bull. 122, 1192 – 1208, doi: 10.1130/B30035.1.

Figure captions

Fig. 1. Shaded relief map of central-southwestern Taiwan and the location of the Alishan area (in the rectangle). Inset shows the geographic position of Taiwan with hill/mountain areas shaded.

Fig. 2. Geological map of the Alishan area, modified from Chinese Petroleum Corporation (1986). For location see Fig. 1. Strike/dip data in red are surveyed in this study. Also shown are current tectonic uplift rates based on 2000 – 2008 precise leveling data (Ching et al., 2011). Note the two negative rates (in red) apparently reflecting mass wasting.

Fig. 3. Contoured, shaded-relief map of the Alishan area, constructed by 40-m mesh DEM issued by the Ministry of the Interior (based on data around 1980s). For location see Fig. 1. Contour intervals at 10 m. T: Tashan surface (undifferentiated); S1 – S5: Alishan surface. Circled is a beheaded valley on the main drainage divide. Arrows point to east-striking linear escarpments truncating Surfaces S4 and S5. Also exhibited are locations of benchmarks for leveling surveys and sites where lateritic soils/colluvium cropped out.

Fig. 4. Topography of the Alishan area. (a) Google Earth 3-D satellite image (date: 2 December 2015), no vertical exaggeration. White arrow points to train station; blue arrow denotes the downstream-most course of tributary (see also Fig. 3).

760 Note that the 2009 Erhwanping landslide (between Erhwanping and Pingthena
761 train stations) has been remediated by engineering works. (b) Transverse profile
762 trending N34°W, with Mt. Tashan and Mt. 2361 included. Rock formations in
763 Fig. 2 are shown, with diagonal lines signifying generalized bedding planes.
764 **Fig. 5.** Scenes of Alishan. (a) The broadest gentle slope (Surface S1). Viewed to the
765 west (from the Mianyue railway); yellow arrow points to Alishan train station.
766 The 2009 Erhwanping landslide in the distance; white arrow shows the moving
767 direction. (b) Surface S1 and its bounding escarpment, viewed to the east (from
768 the western flank of the Erhwanping landslide). Yellow line on the escarpment
769 traces the bedrock bedding plane below colluvium. (c) The Tashan cliff, viewed
770 from Erhwanping train station. (d) The Tashan cliff and the 2009 Datashan
771 landslide, viewed from the Alishan forest recreation park. Arrow points to the
772 rock shed tunnel of the Mianyue railway.
773 **Fig. 6.** The 2009 Erhwanping landslide, viewed from Mt. Tashan (taken on August,
774 2012). For location see Fig. 3. Arrows point respectively to Erhwanping and
775 Pingthena train stations, which have a relief of ~280 m. Terrace I was created
776 during 2009 Typhoon Morakot. Sites of radiocarbon dates with ages are also
777 shown (see also Fig. 7).
778 **Fig. 7.** Summary of stratigraphic and chronological data in this study (see also Table

779 1). For map location and legend see Fig. 3. Arrows below Mt. Tashan point to
780 remnants of gentle, colluvial slopes preserved at the lower part of the cliff.
781 Radiocarbon dates (in red) >40 ka are expressed as conventional radiocarbon
782 ages (unit: BP). Those <7 ka are converted to 1σ calibrated age ranges (unit: cal
783 BP). Heights of stratigraphic columns (in meter) are relative to tributary riverbeds
784 except No. 8, 10, 14 – 17 which are relative to the trunk riverbed.

785 **Fig. 8.** Reddish colluvium exposed around Landslide X (for location see Figs. 3 and
786 7). (a) Along the road crossing the landslide scarp. (b) A close view of the
787 road-cut outcrop, showing the mixture of yellowish gravel clasts with reworked
788 lateritic soils. (c) A sliced lateritic sandstone cobble, which can easily be scraped
789 across the concrete road to produce red-colored streaks. (d) A mixture of
790 yellowish, brownish, and reddish colluvial gravels exposed where the landslide
791 cut Surface S2.

792 **Fig. 9.** Colluvium underlying Alishan surface (for location see Fig. 7). All taken in the
793 summer of 2012. (a) Below the Erhwanping train station (Site 1). The retaining
794 wall (~30 m high) and other slope works were constructed after 2009 Typhoon
795 Morakot. (b) Below the slope ~160 m high above Pingthena train station (Site 2),
796 a distant view. (c) Site 2, a relatively close view. Note a subrounded giant
797 bounder (labelled G) nearly 10 m in diameter. (d) A close view of the greyish

gravel in (c). Arrows point to non-carbonized wood fragments. (e) Along the left bank of Tributary B (Site 6). (f) Along a tributary of the Tsengwen River cutting Surface S3 (Site 7). A hammer (circled) for scale.

Fig. 10. Longitudinal profile of the Alishan River from headwaters to Laichi, based on 40-m mesh DEM issued by the Ministry of the Interior (based on data around 1980s). Sedimentary/topographic features are summarized. The outer edges of Surfaces S1 and S2, and the inner edges of the gentle-slope remnants shown in Fig. 7 are also projected.

Fig. 11. Topographies of the Alishan River. All taken in the summer of 2012 or in early 2013. (a) Step-pool topography along the uppermost part of the river above the junction with Tributary A. (b) Piles of giant boulders upstream of the mouth of Tributary A. Boulders are generally >2 m and up to several meters in diameter. (c) Deep valley around the mouth of Tributary B, which forms a waterfall ~50 m high. Arrow points to the trace of bedrock bedding plane below colluvium. (d) Waterfall (pointed) upstream of the junction with Tributary C. (e) Gorge downstream from the junction with Tributary C (facing downstream). (f) Remnant of gentle, colluvial slopes (pointed) above the gorge (see also Fig. 7 for location). Viewed from Erhwanping landslide.

Fig. 12. Colluvium exposed along the Alishan River (for location see Fig. 7). (a)

817 Colluvial gravel ~50 m thick underlying Terrace T (Site 9). Yellow arrow points
818 to the boundary between the lower, greyish gravel (massive) and the upper,
819 grayish/yellowish gravel (stratified). (b) A typical view of the lower greyish
820 gravel in (a), with a piece of non-carbonized tree trunk (dated 41,935±799 BP). (c)
821 Greyish gravel exhibited downstream of the junction with Tributary A (Site 10;
822 left bank). (d) Greyish gravel exposed along Tributary D (Site 14).
823 **Fig. 13.** Young sediments exposed along the gorge part of the Alishan River and
824 around Landslide Y (for location see Fig. 7). (a) A distant view of a toppled log
825 (indicated by arrow), which is included in a bed of slackwater sand stranded ~50
826 m high above the valley bottom (Site 16). Two people are circled for scale. (b) An
827 upward view of a >50-m thick colluvial sequence at Site 17. A person is circled.
828 (c) Grayish colluvial gravel exposed along the eastern flank of Landslide Y. (d)
829 Landslide Y, taken on January, 2013. LD = landslide deposit. DT = debris terrace
830 constructed by debris flows generated during 2009 Typhoon Morakot. Arrow
831 points to the location of the profile in (c).
832 **Fig. 14.** Schematic diagrams showing the inferred temporal change in river/hillslope
833 processes in the study area undergoing tectonic uplift. (a – c) During the wet
834 last-interglacial period. Downward river incision dominated and most sediments
835 yielded from hillslopes were able to be conveyed downstream. (d, e) During the

dry last-glacial period. Valley aggradation dominated due to low erosion/transport capacity of rivers. (f) During the wet postglacial period. Rapid river incision resumed and the previously accumulated colluvium started to be flushed out of valley.

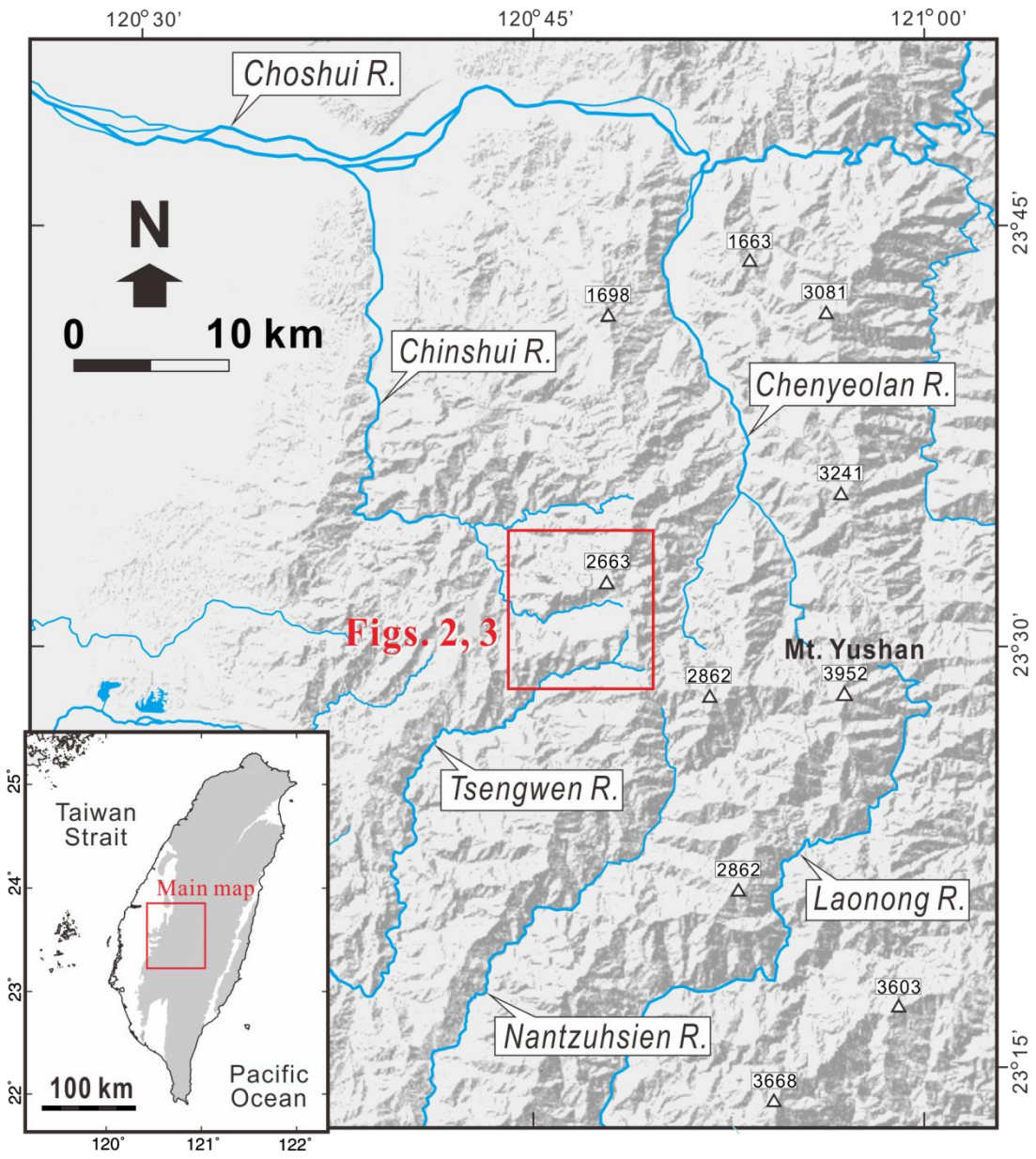

841

842 (Fig. 1)

843

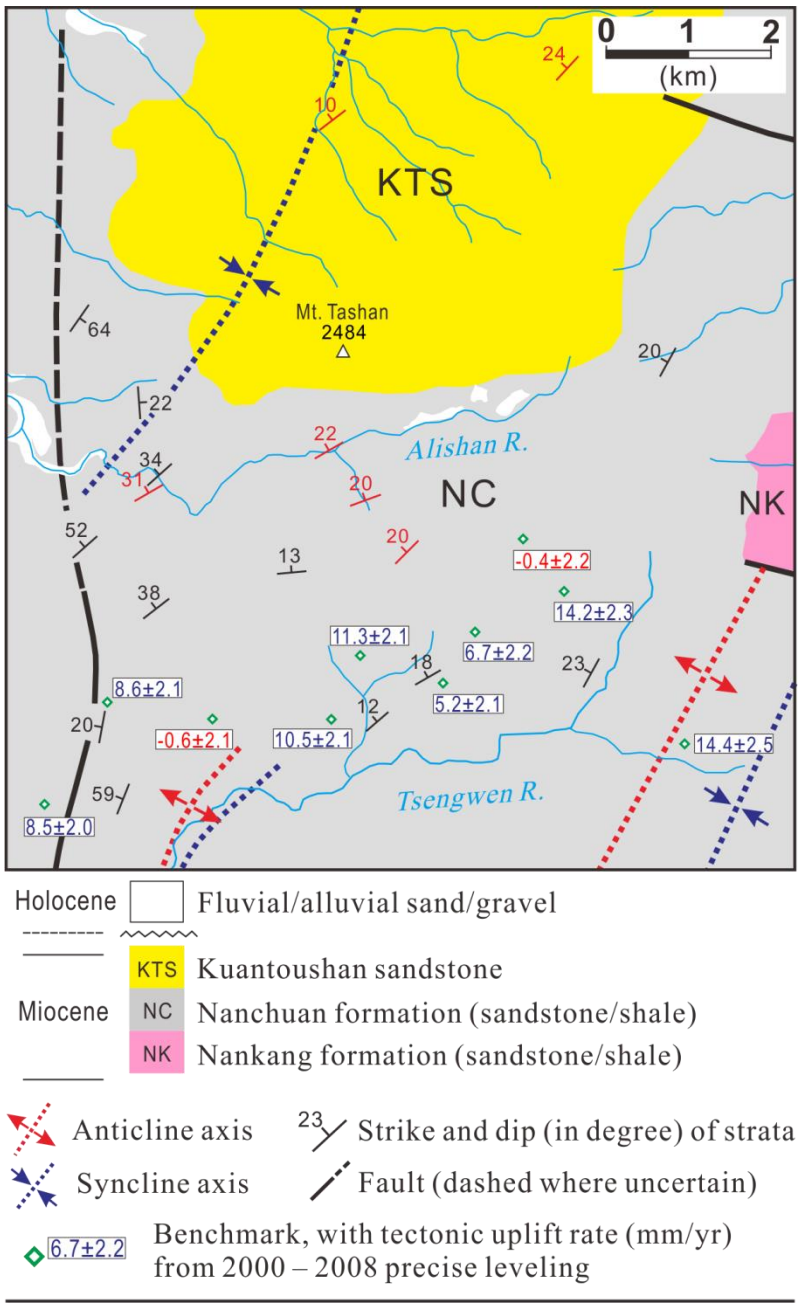

844

845 (Fig. 2)

846

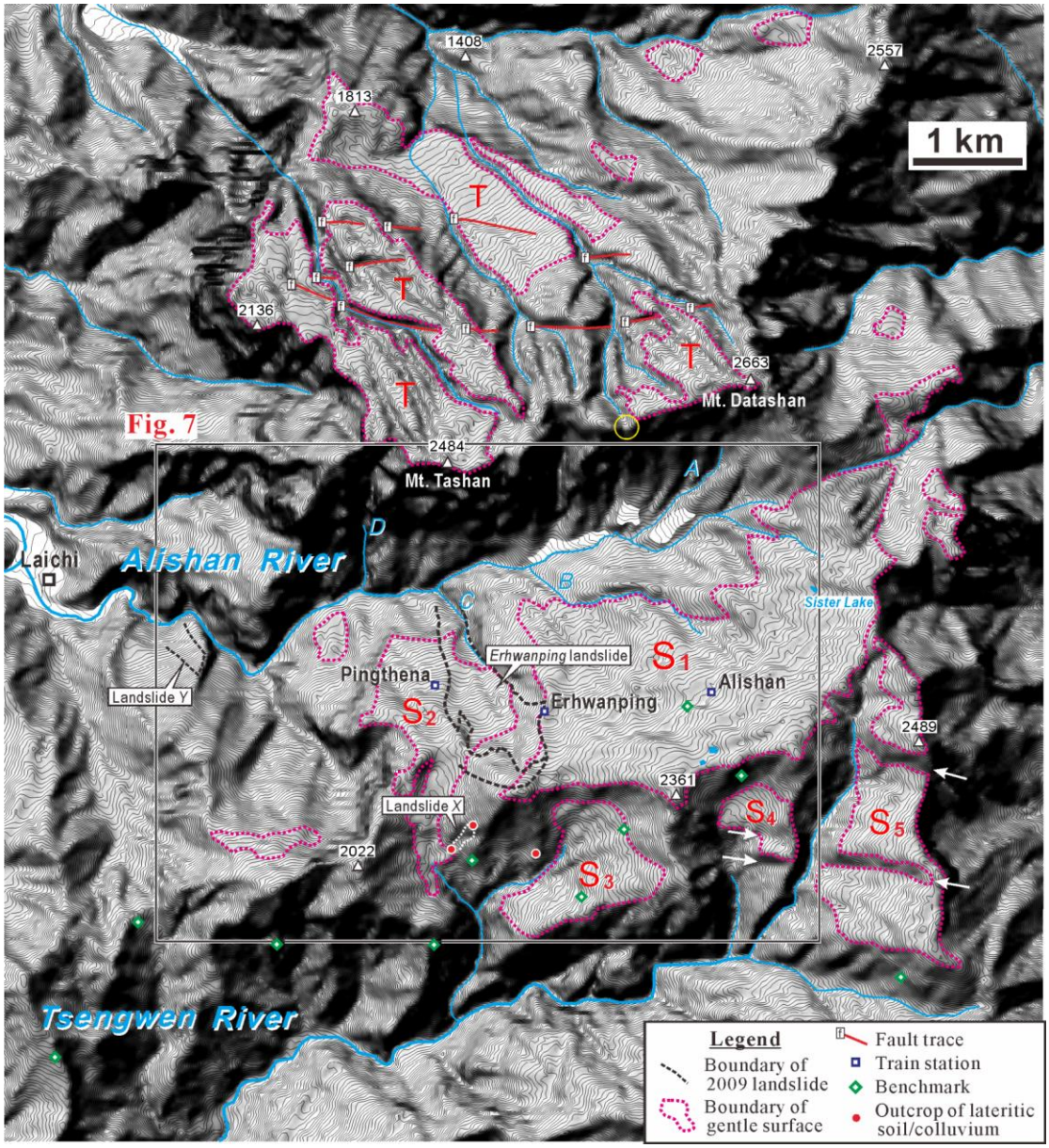

847

848 (Fig. 3)

849

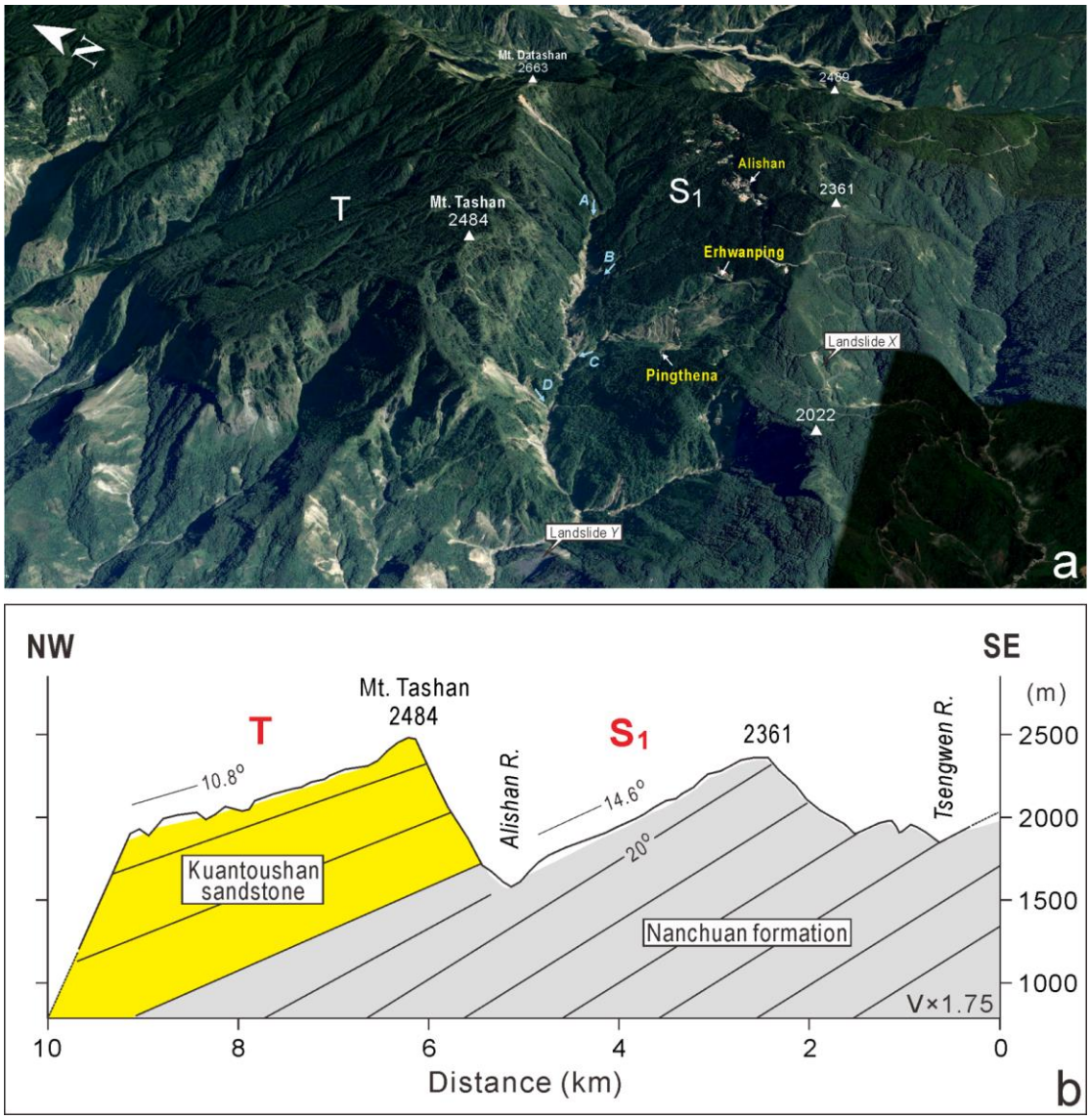

850

851 (Fig. 4)

852

853

854

855 (Fig. 5)

856

857

858 (Fig. 6)

859

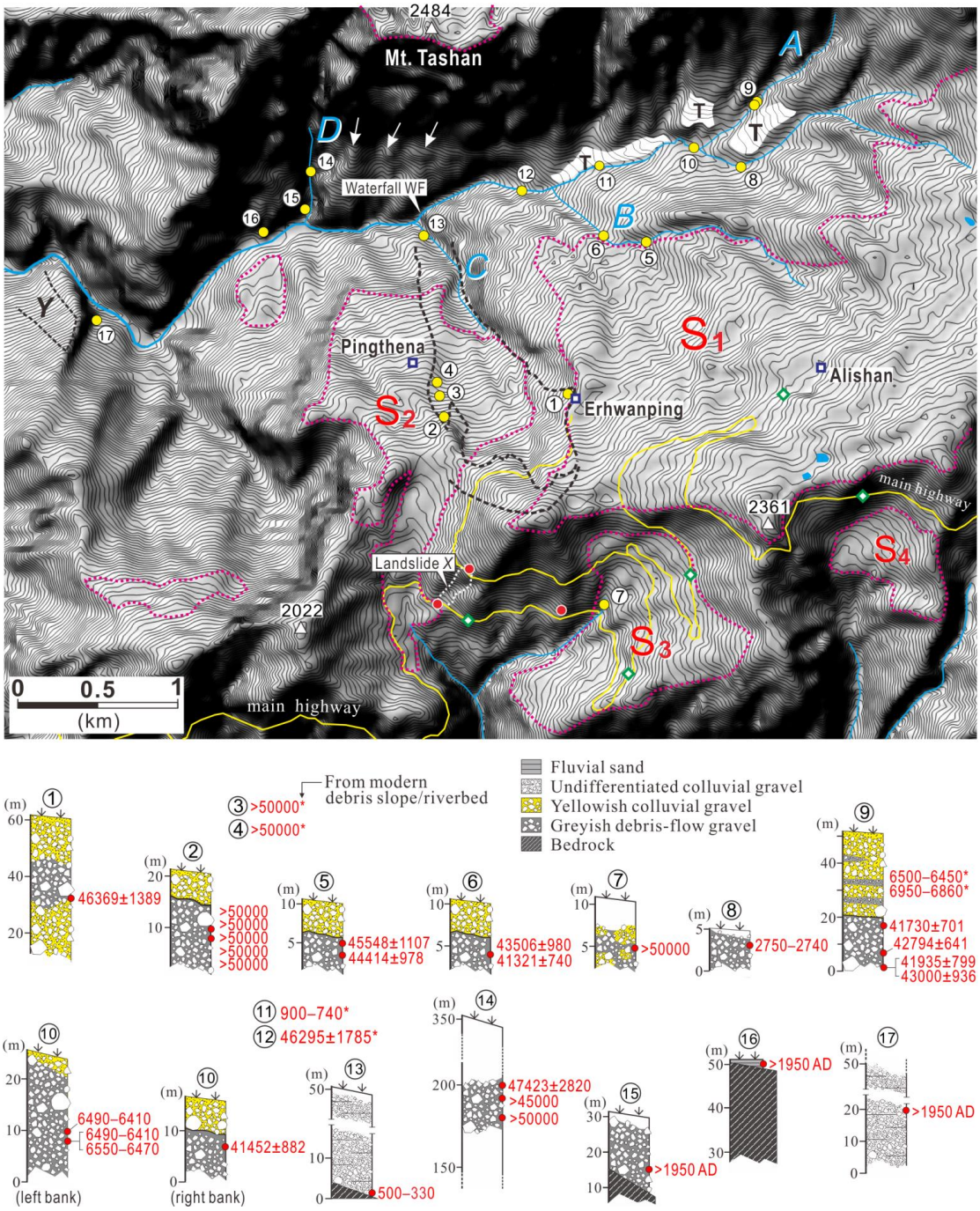

860

861 (Fig. 7)

862

(Fig. 8)

(Fig. 9)

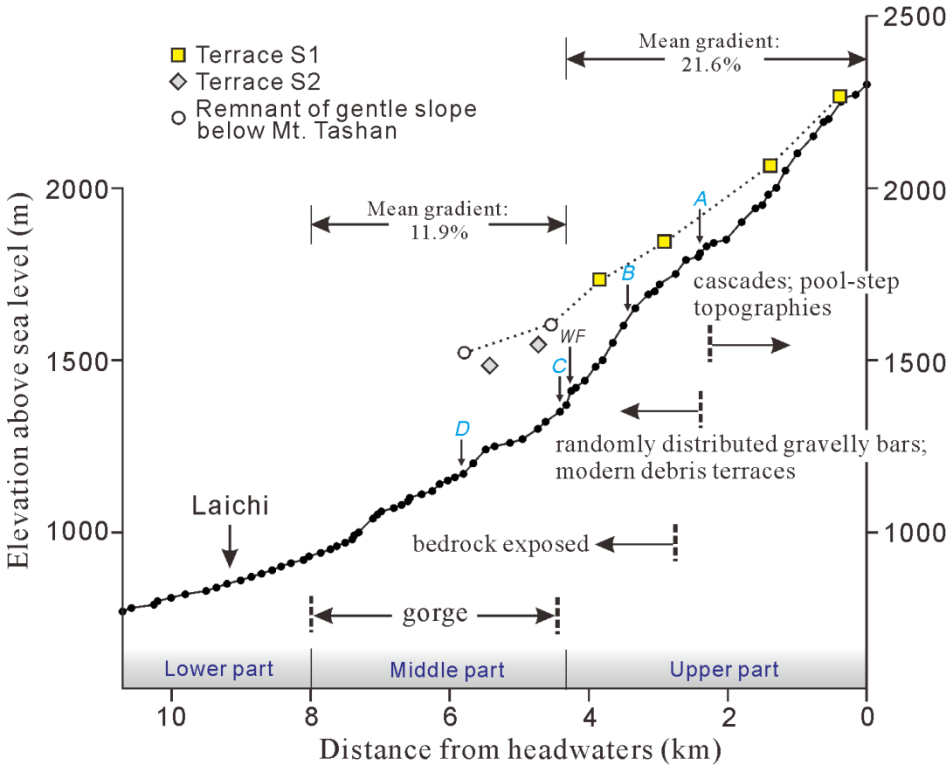

869

870 (Fig. 10)

871

(Fig. 11)

875

876 (Fig. 12)

877

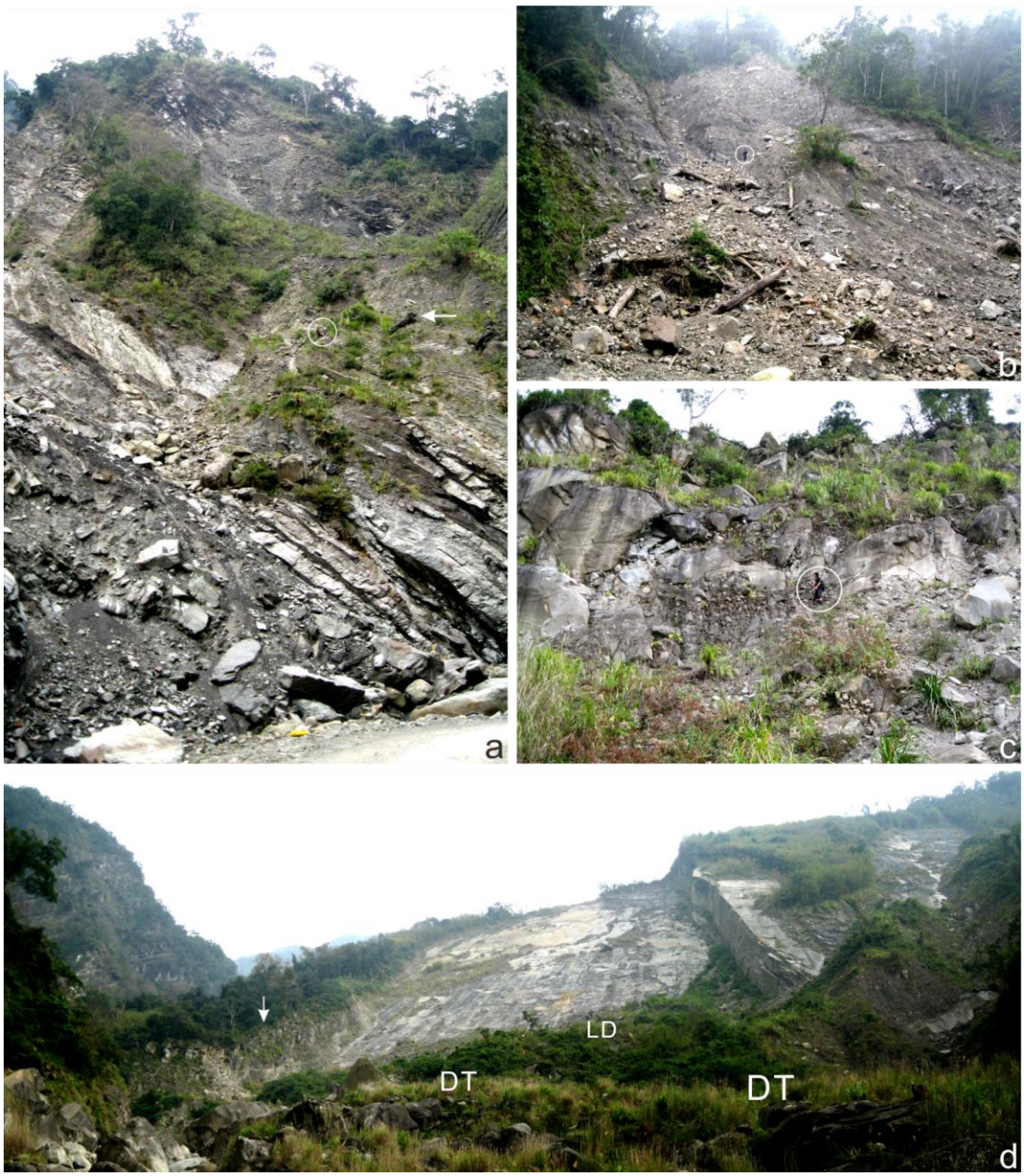

878

879 (Fig. 13)

880

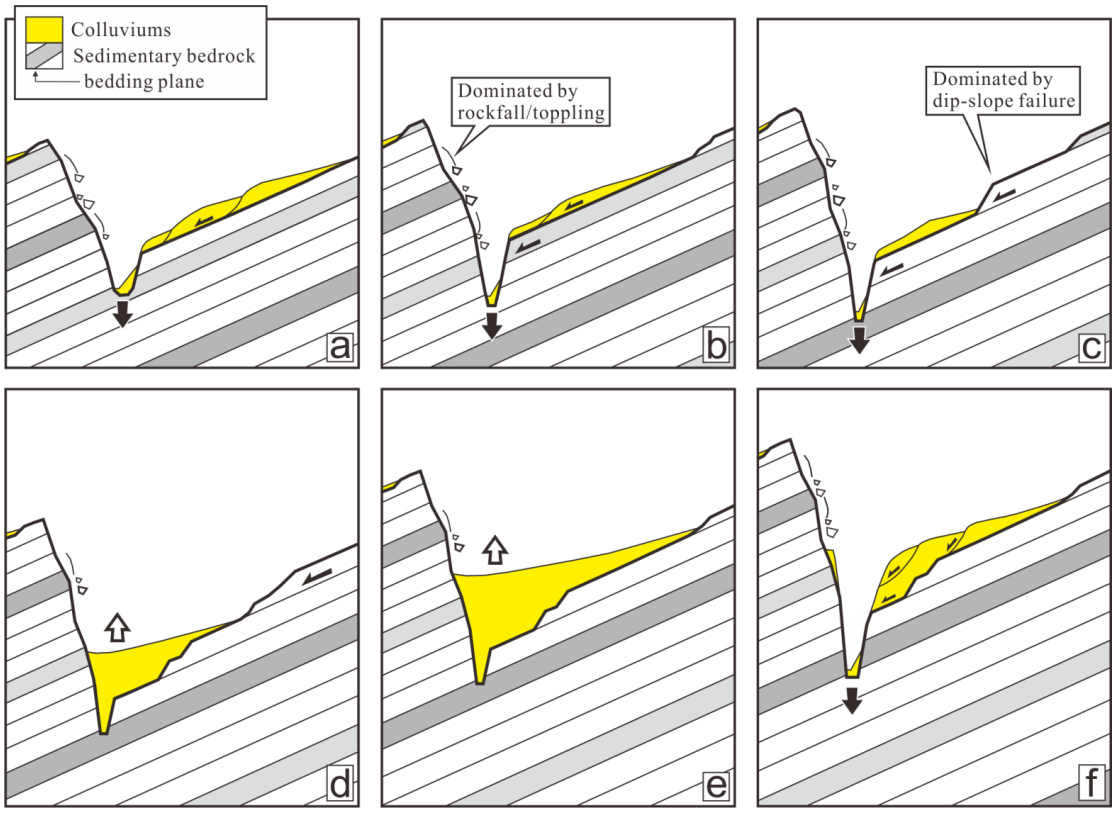
Colluviums
Sedimentary bedrock
bedding plane
Dominated by rockfall/toppling
Dominated by dip-slope failure
a
b
c
d
e
f

(Fig. 14)